

Immobilization of Molecular Catalysts on Solid Supports via Atomic Layer Deposition for Chemical Synthesis in Green Solvents

Pooja J. Ayare[#], Shawn A. Gregory[†], Ryan J. Key[#], Andrew E. Short[†], Jake G. Tillou[#], James D. Sitter[#], Typher Yom[†], Dustin W. Goodlett[#], Dong-Chan Lee[†], Faisal M. Alamgir[†], Mark D. Losego^{†*}, and Aaron K. Vannucci^{#*}

[#]Department of Chemistry and Biochemistry, University of South Carolina, Columbia, SC 29208, USA

[†]Department of Materials Science & Engineering, Georgia Institute of Technology, Atlanta, GA 30332, USA

*corresponding author: vannucci@mailbox.sc.edu losego@gatech.edu

Abstract

Homogeneous molecular catalysts are valued for their reaction specificity but face challenges in manufacturing scale-up due to complexities in final product separation, catalyst recovery, and instability in the presence of water. Heterogenizing these molecular catalysts, by attachment to a solid support, could transform the practical utility of molecular catalysts, simplify catalyst separation and recovery, and prevent catalyst decomposition by impeding bimolecular catalyst interactions. Previous strategies to heterogenize molecular catalysts via ligand-first binding to supports have suffered from reduced catalytic activity and leaching (loss) of catalyst, especially in environmentally friendly solvents like water. Herein, we describe an approach in which molecular catalysts are first attached to a metal oxide support through acidic ligands and then “encapsulated” with a metal oxide layer via atomic layer deposition (ALD) to prevent molecular detachment from the surface. For this initial report, which is based upon the well-studied Suzuki carbon-carbon cross-coupling reaction, we demonstrate the ability to achieve catalytic performance using a non-noble metal molecular catalyst in high aqueous content solvents. The catalyst chosen exhibits limited catalytic reactivity under homogeneous conditions due to extremely short catalyst lifetimes, but when heterogenized and immobilized with an optimal ALD layer thicknesses product yields > 90% can be obtained in primarily aqueous solutions. Catalyst characterization before and after ALD application and catalytic reaction is achieved with infrared, electron paramagnetic resonance, and X-ray spectroscopies.

Introduction

Molecular transition metal catalysts in homogeneous solutions tend to exhibit high catalytic activity and reaction selectivity, but also exhibit poor stability and short lifetimes.¹ One major pathway to molecular catalyst deactivation is the formation of off-cycle intermediates via intermolecular catalyst interactions. While catalyst dimers or trimers are sometimes necessary for catalytic activity,² most catalyst “multi”-mers result in catalytic dead ends.³⁻⁵ Multimer formation is often promoted by water in the reaction solution, as shown in Figure 1A,^{3, 6, 7} thus limiting the ability to utilize highly environmentally safe solvents. One common approach to minimizing intermolecular catalyst interactions is to perform catalytic reactions under very low catalyst loadings.⁷⁻¹⁰ This approach has led to impressively high initial turnover frequencies (TOFs) but often times does not appreciably increase catalyst lifetimes.⁷

The immobilization of molecular catalysts onto solid supports is an approach designed towards preventing intermolecular catalyst interactions and extending molecular catalysts lifetimes.¹¹ The isolation of molecular catalysts on solid supports inhibits bimolecular catalyst interactions and thus takes advantage of the inherent catalyst activity. This approach of creating a molecular/heterogeneous catalyst has the added benefits of increased solvent compatibility, increased ease of catalyst separation from reaction mixtures, possible incorporation into flow reactors, and potential for catalyst recycling.^{6, 12} This approach, however, can have its own set of drawbacks including increased cost of catalyst synthesis, possible decreases in catalyst selectivity, and difficulty in preventing catalyst leaching from the solid support.¹³ The increased cost of both the materials and catalyst preparation can be overcome by achieving previously unattainable reactivity through extending catalyst lifetimes and recyclability.

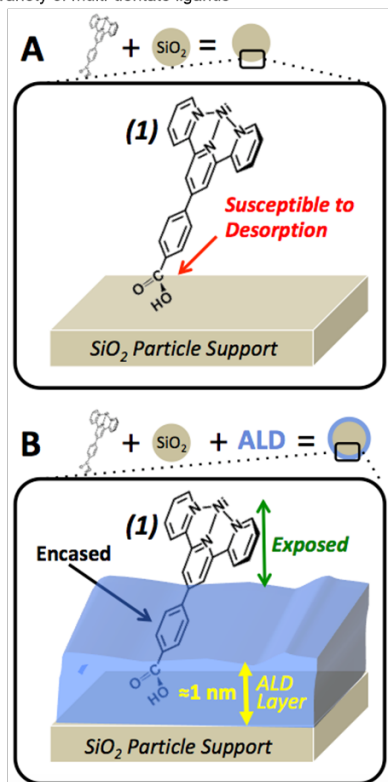
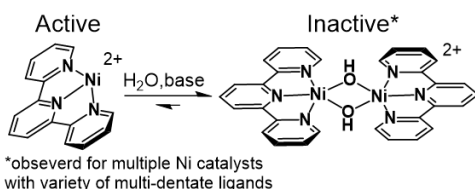


Figure 1: Comparison of previous work to current study. A. Example of molecular nickel catalyst deactivation in homogeneous solution. B. Depiction of molecular catalyst (1) loaded onto an SiO₂ support susceptible to desorption and subsequent deactivation. C. This work, stabilization of molecular catalyst with an ALD encapsulation layer.

Extensive research has been reported on immobilized catalysts in the field of surface organometallic chemistry (SOMC). This approach generates individual catalyst molecules on solid oxide supports through direct binding of transition metals to the oxide supports. This binding occurs after a thorough preparation of the oxide surface to create sites capable of strong binding to individual metal atoms.¹⁴ The metal atoms that bind the oxide support can be introduced to the support through solution phase chemistry¹⁵ or directly via ALD methods.¹⁶ Many of these SOMC catalysts are composed of early transition metals due to their oxophilicity,¹⁷ but recent reports have extended SOMC to the late transition metals.¹⁸⁻²¹ An impressive array of catalytic transformations has been achieved with this class of SOMC catalyst.^{22, 23} Similar to polymer-supported²⁴⁻²⁶ and MOF-supported^{27, 28} catalysts, SOMC catalysts utilize the support as a ligand for the catalysts, therefore, there is no direct analogous homogeneous catalysts for comparison. Iterative design of SOMC catalysts, hence, cannot directly benefit from homogeneous catalyst studies.

Ligand-first binding of molecular catalysts to a support is an alternative approach to catalyst immobilization on solid metal oxides that could benefit from previous understandings of homogeneous catalysis. The ligand-first class of molecular/heterogeneous catalysts on oxide supports is inspired by the

design of dye sensitized solar cells,²⁹⁻³² and electrocatalysis.³³⁻³⁵ In this approach catalytic activity and selectivity of homogeneous catalyst can often be translated to the molecular/heterogeneous system.^{36, 37} Furthermore, the lifetimes of homogeneous catalysts that rapidly deactivate in solution through bimolecular routes such as dimerization, may have their lifetimes greatly enhanced by isolation on a solid support as illustrated in Figure 1B. However, detachment of ligand-first molecules from metal oxide supports remains a problem.^{13, 36-38} Detachment, or leaching, of the molecular catalysts into solution is typically promoted by water or highly polar organic solvents disrupting the ligand binding to the support. Metal oxide supports can even accelerate decomposition and nanoparticle formation of leached molecular catalysts.¹³ Many strategies for increasing the binding strength between molecular catalysts and metal oxide surfaces have been explored.^{35, 39} While these binding motifs have been successful to varying degrees, most still have limited stability under reaction conditions, especially in the presence of water.^{40, 41}

Herein, we describe a potentially universal method for reliably attaching and isolating molecular catalysts ligand-first to solid metal oxide supports for solution-based chemical catalysis. This paradigm uses atomic layer deposition (ALD) to physically encapsulate pre-bound molecular catalysts to solid metal oxides. ALD allows for precise control of oxide layer growth and has been used to isolate single-site heterogeneous catalysts.^{42, 43} As shown in Figure 1C, this precise control allows for encasing the hybrid catalyst binding sites while leaving the catalyst active site exposed to solvent and substrate. The ALD layer thus immobilizes and strongly adheres the molecular catalyst onto the solid oxide support. This immobilization generates a hybrid single molecule catalyst and allows for the use of green, polar solvents, such as water. It is worth noting, that cross-coupling reactivity with nickel catalysts in water has been achieved with the addition of micelles in the reaction solution.^{44, 45} In addition, this approach allows for the use of nickel-based catalysts for reactions that are typically performed by palladium.^{46, 47} Both the ACS Pharmaceutical Round Table and the Green Chemistry Institute have called for increased use of nickel catalysts in cross-coupling reactions,⁴⁸ however, nickel catalysts are not being widely employed in the fine chemical industry.⁴⁹ Controlled reactivity, catalyst stability, and batch-to-batch consistency of nickel catalysts is still lacking. Often nickel catalysts exhibit a high degree of sensitivity to the choice of solvent, base, moisture levels, and substrates employed during coupling reactions. The ALD immobilization of molecular nickel catalysts onto solid supports has been designed to overcome these shortcomings and create a general catalyst motif for use in fine chemical synthesis.

This approach builds upon our prior work that used ALD to attach active molecular photosensitizers to nanostructured electrodes for photoelectrochemical devices.^{12, 50-52} However, in those systems, device performance required careful design of ALD encapsulation layers that permitted proper electron transfer between molecule and oxide support. For chemical catalysis, this requirement is no longer necessary, simplifying the design. Moreover, as shown here, attachment of molecular catalysts to solid supports can lead to new reactivity not seen under homogeneous conditions. Most approaches to molecular catalyst immobilization involve developing, or taking from literature, successful homogeneous catalysts and attempting to adapt them for use as immobilized catalysts on heterogeneous supports. Poor homogeneous catalysts, however, are rarely considered for immobilization. Many poor homogeneous catalysts only suffer from very short catalyst lifetimes due to being susceptible to the catalyst deactivation pathways discussed above (e.g., dimerization). Deactivation through routes such as dimerization should be less likely, or even completely prevented when catalysts are immobilized. Herein, we show that immobilization via ALD of a poor homogeneous molecular catalyst significantly extends its lifetime as a hybrid heterogeneous catalyst for chemical synthesis. Thus, using ALD to create hybrid catalysts via immobilization of molecular catalysts without concern for their homogeneous reactivity opens a new approach and chemical space for catalyst discovery. As a demonstration, we report the design and synthesis of a hybrid nickel catalyst using ALD, characterize the synthesis steps with spectroscopic techniques, and show proof-of-concept Suzuki

cross-coupling reactions to illustrate consistent catalytic activity in green solvents with high aqueous content.

Results and Discussion

We recently reported on the design and catalytic testing of a molecular/heterogeneous nickel catalyst.⁶ The catalyst in Figure 1B was composed of a molecular terpyridine nickel catalyst bound to a solid SiO₂ support through a carboxylic acid linker. This molecular/heterogeneous catalyst exhibited prolonged catalyst lifetimes for Suzuki cross-coupling using dioxane as the solvent for the coupling partners, in addition the benefits of utilizing terpyridine ligands for nickel catalysts have also been explored.⁵³ The analogous homogeneous molecular catalyst quickly dimerized and became catalytically inactive. A series of control reactions and characterization of the molecular/heterogeneous catalyst pre- and post-reaction strongly supported the surface-bound catalyst being the active catalyst for cross-coupling reactivity. This molecular/heterogeneous catalyst, however, still required the toxic organic solvent dioxane to operate. Attempts to achieve cross-coupling reactivity in green solvents such as ethanol and water were unsuccessful. These failures were attributed to the protic, polar solvents disrupting catalyst binding to the SiO₂ support, resulting in desorption of the catalyst from the surface. Upon catalyst desorption, the molecular catalyst in solution quickly dimerized and deactivated. In this report, ALD is utilized (Figure 1C) to overcome the previously observed catalyst deactivation and perform catalytic chemical synthesis in solvents containing a high-volume ratio of water.

Synthesis of 1|SiO₂|TiO₂

The molecular catalyst [(2,2':6',2''-terpyridine-4'-benzoic acid)Ni(II)]Cl₂ (**1**) was synthesized following a previously reported procedure.⁶ Loading of **1** onto Aerosil A300 SiO₂ support to form **1|SiO₂** (Figure 1B) followed a one-step method also previously reported.⁶ Catalyst **1|SiO₂** was characterized before atomic layer deposition to examine how ALD may affect the structure or binding of **1** to the SiO₂ support. ICP-MS analysis indicates that **1|SiO₂** contains 0.4 weight% nickel pre-ALD treatment, which equates to roughly 2×10^{-7} mols of catalyst per m² of support surface area. In addition, elemental analysis from scanning transmission electron microscopy - energy dispersive spectroscopy (STEM-EDS) confirmed nickel was present on the SiO₂ particles (Figure S2). X-ray diffraction (XRD) analysis of **1|SiO₂** (Figure S1) does not show any evidence for crystalline nickel particles, suggesting that the molecular nickel catalyst, not metallic nickel or nickel oxide particles, are present on the SiO₂ support pre-ALD treatment. Infrared attenuated total reflection (FTIR-ATR) spectroscopy was used to characterize the ligand binding to the support. The left-hand side of Figure 2 shows the comparison of the FTIR of the molecular catalyst **1** (Fig. 2A) to the FTIR-ATR of **1|SiO₂** (Fig. 2C). The molecular catalyst **1** has a prominent C-O stretching frequency at 1729 cm⁻¹. Upon attachment of **1** to the SiO₂ support to form **1|SiO₂**, this prominent C-O stretching frequency remains present but shifts to 1636 cm⁻¹. This shift is consistent with carboxylate binding to metal oxide supports as has been previously observed.^{54, 55}

Catalyst **1|SiO₂** was then immobilized using TiO₂ ALD (10 cycles of TiCl₄ + H₂O as described in the experimental section). The ALD procedure was designed to coat **1|SiO₂** with a ~1.0 nm thick layer of TiO₂ to create the hybrid catalyst **1|SiO₂|TiO₂** as depicted in Figure 1C. ICP-MS analysis reveals that **1|SiO₂|TiO₂** catalyst contains 0.35 weight% nickel, indicating minimal, if any, loss of nickel catalyst during ALD. We mainly attribute the lower weight% nickel to the increased weight of the solid catalyst with the addition of the TiO₂ layer. STEM-EDS analysis on **1|SiO₂|TiO₂** also detected the presence of Ni and Ti as expected (Figure S3). XRD analysis of **1|SiO₂|TiO₂** again shows no evidence for nickel nanoparticles (Figure S1) nor were any nanoparticles ever observed with STEM imaging (SI). The FTIR-ATR spectrum of **1|SiO₂|TiO₂**, plotted in Figure 2B, continues to show the existence of the C-O stretching frequencies that are indicative of carboxylate binding to metal oxides. No measurable shift in the C-O stretching frequencies

between **1**|SiO₂ and **1**|SiO₂|TiO₂ suggests that the ALD treatment did not significantly alter the binding of the ligand to the SiO₂ support.

To investigate the stability of the nickel center of the catalyst, electron paramagnetic resonance (EPR) spectroscopy was utilized as shown on the right-hand side of Figure 2. The EPR spectrum shown in Figure 2E is that of a solid sample of the molecular catalyst **1** obtained at room temperature. The spectrum in Figure 2D is of catalyst **1**|SiO₂|TiO₂ catalysts after ALD coatings. The similar spectral splitting and shifts indicates the nickel centers between the two samples (**1** and **1**|SiO₂|TiO₂) have the same oxidation-states and chemical binding environment. For comparison, the EPR spectrum of nickel oxide on SiO₂ support is shown in Figure 2F. Nickel oxide particles exhibit a clearly distinct EPR spectrum, and the data in Figure 2 taken as a whole, indicate the molecular nickel catalyst is stable and maintains molecular integrity throughout the ALD coating process. Differences in reactivity between **1**|SiO₂ and **1**|SiO₂|TiO₂ as discussed in the next section lend further support for the structure of **1**|SiO₂|TiO₂ proposed here (*vide infra*).

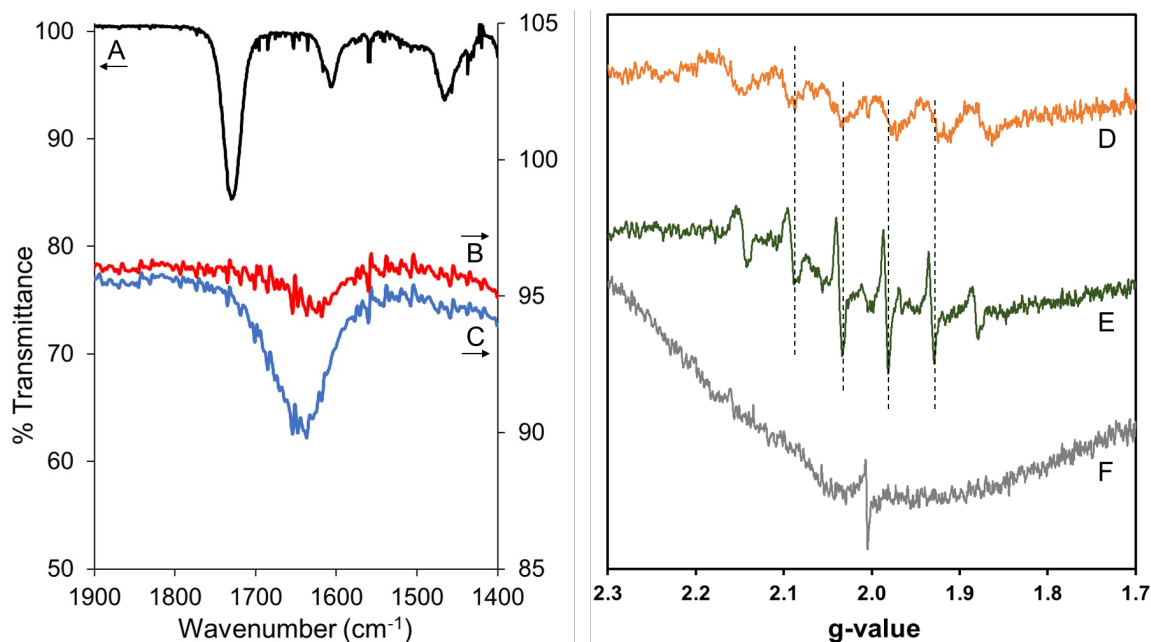
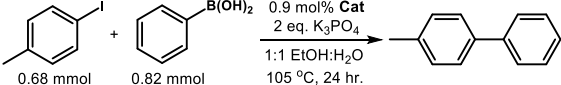
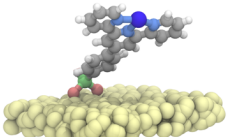
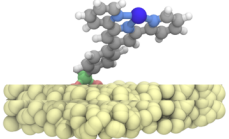
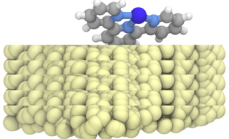
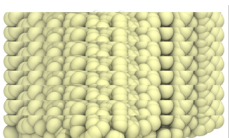


Figure 2. Overlay of FTIR-ATR spectra (left) and EPR spectra (right). FTIR: A (black) molecular catalyst **1**. B (red) **1**|SiO₂|TiO₂. C (blue) **1**|SiO₂ (C, blue). ERP: D (orange) **1**|SiO₂|TiO₂. E (brown) molecular catalyst **1**. F (grey) nickel oxide on SiO₂ support.

Catalytic Performance

To illustrate the advantage of this hybrid ALD catalyst approach, and to determine the optimized ALD layer thickness, a series of catalytic Suzuki cross-coupling reactions were performed. Table 1 presents the results of these test reactions along with illustrations of the proposed ligand-first bound catalyst compositions. The reaction shown in Table 1 was chosen as a simple test reaction to determine the optimal conditions and catalyst composition. The reaction conditions were chosen to highlight the green chemistry possibilities of this catalytic system. For solid support hybrid catalysts, 0.9 mol% nickel catalyst was used per reaction with respect to the limiting reagent iodotoluene. The solvent system chosen was a 1:1 ratio of ethanol and water, with the ethanol serving to help increase the solubility of the organic substrates. The only reaction additive was K₃PO₄ base, where base is a mechanistic requirement for boronic acid activation.⁵⁶ Lower reaction temperatures (80 °C) and shorter reaction times (12 hrs.) resulted in lower yields than compared to the optimal reaction temperature and time (105 °C and 24 hrs).

Table 1. Determining optimal ALD layer thickness for cross-coupling reactions in ethanol:water solvent.

	
Cat	Yield
1	0%
 1 SiO₂	5%
 1 SiO₂ with 0.5 nm TiO₂ ALD	32%
 1 SiO₂ with 1.0 nm TiO₂ ALD (1 SiO₂ TiO₂)	90%
 1 SiO₂ with 1.5 nm TiO₂ ALD	2%

The results in Table 1 indicate that the optimal catalyst design consists of **1** attached to a SiO₂ support with approximately 1.0 nm thickness of TiO₂ applied via 10 ALD cycles (**1|SiO₂|TiO₂**). For molecular catalyst **1** in homogeneous solution, no product formation was detected. This result is due to rapid catalyst dimerization and deactivation promoted by water (Figure 1A). The dimer, [(μ-X)Ni(tpy)]₂ where X = Cl⁻ or OH⁻, has been shown to be inactive for this catalytic transformation.⁶ The molecular catalyst **1** attached to an SiO₂ support without applied ALD layers (**1|SiO₂**), is able to generate product at a 5% yield, and post reaction analysis of **1|SiO₂** with ICP-MS revealed that the solid support no longer contained any detectable nickel. Thus, without an ALD layer, the polar ethanol water solvent mixture promotes the detachment of the molecular nickel catalyst from the surface of the SiO₂ support and the catalyst then deactivates in solution. A thin layer (less than 1 nm, see experimental section) of TiO₂ was then applied to the **1|SiO₂** structure via 5 ALD cycles and this catalyst produced the cross-coupled product with 32% yield. This non-optimal yield suggests that “thin” ALD layers are insufficient to fully protect the catalyst binding sites from solvent attack and subsequent desorption. The reason for incomplete protection is not entirely clear, but it is likely due to either poor coating uniformity at these thicknesses (i.e., nucleation delay) or simply insufficient thickness to block attack of the binding groups by the polar solvent.

Next, a roughly 1 nm layer of TiO₂ was applied to the **1|SiO₂** structure via 10 ALD cycles to yield catalyst **1|SiO₂|TiO₂**. As can be seen in Table 1, the 10 ALD cycle layer results in a catalyst capable of

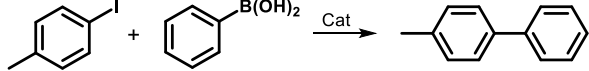
achieving optimal yields of the desired product. Computations on the Pd analogue of **1**, calculated a distance between the C atom of the COOH group and the metal center was nearly 1.2 nm,⁵⁷ indicating that an average 1 nm thick ALD layer would still expose the Ni center to the reaction solution. Post reaction ICP-MS indicates that 0.31 wt% nickel remained on the **1**|SiO₂|TiO₂ catalyst, indicating that minimal nickel loss during the 24 hr reaction. ICP-MS analysis of the reaction solution post reaction did detect 1.77 µg of nickel per gram of solution. This minimal nickel in solution could occur due to nickel loss from the tpy ligand and not from complete molecular catalyst desorption from the surface of the oxide support. EDS analysis of the post-reaction catalyst also detected the continued presence of Ni and Ti on the SiO₂ surface (Figure S5), and an elemental map showed highly dispersed Ni on the surface with no evidence of nanoparticle formation (Figure S6), supported by XRD patterns (Figure S1). In addition to the detected Ni and Ti, the STEM-EDS analysis shows potassium and phosphorous content on the surface, likely arising from the K₃PO₄ base used during the reaction. FTIR-ATR analysis of the solid molecular/heterogeneous catalyst post reaction also showed C-O stretching frequencies assigned to the ligand binding to the oxide support (Figure S4).

These results suggest that the 10 ALD cycle TiO₂ layer now sufficiently coats the SiO₂ surface, fully immobilizing the molecular catalyst by stabilizing the ligand COOH binding to the oxide surface. This stabilized ligand binding prevents catalyst desorption and protects the catalyst from bimolecular degradations. Furthermore, BET analysis of **1**|SiO₂ and **1**|SiO₂|TiO₂ indicated that the ALD layer does not lead to an appreciable difference in surface area of the solid support ($216 \pm 0.8 \text{ m}^2/\text{g}$ and $223 \pm 0.8 \text{ m}^2/\text{g}$ respectively, Figures S7 and S8). The surface area analysis implies the ALD uniformly coats the SiO₂ support without clogging the micropores. It is also worth noting that molecular catalyst **1** attached to a TiO₂ support without ALD applied (**1**|TiO₂) did achieve a 38% yield of the cross-coupled product. This indicates the ligand binding to TiO₂ is stronger than to SiO₂, likely due to the higher isoelectric point of TiO₂ compared to SiO₂. The 38% yield from this reaction is considerably lower than optimized yields obtained through ALD coating, indicating that the catalyst does not just migrate to the TiO₂ layers and the binding sites are “buried” by the TiO₂ ALD as depicted in Table 1. Furthermore, post-reaction ICP-MS analysis of the **1**|TiO₂ catalyst revealed that the molecular catalyst **1** detaches from the surface of this support after a single reaction cycle, which is not consistent with catalysts coated with ALD layers (*vide infra*).

Lastly, a 2.0 nm layer of TiO₂ was applied to the catalyst via 20 ALD cycles. This “thick” coating results in almost no yield of the desired product, as shown in Table 1. ICP-MS analysis of the 2.0 nm thick TiO₂ catalyst revealed that the nickel is still present at levels nearly identical to the pre-reaction levels. Therefore, this result supports that ALD layers can be applied that are too thick and thus fully encase the molecular catalyst. This full enclosure of the catalyst strongly binds the catalyst to the surface but also prevents catalyst activity due to preventing the active nickel center from accessing the reaction substrates.

With the optimized ALD layer thickness determined, control reactions were performed to help further identify the active catalyst species. Results from these control reactions are summarized in Table 2. Reaction 1 in Table 2 shows the designed hybrid catalyst **1**|SiO₂|TiO₂ leads to an efficient product yield of 90%. For rxn. 3 in Table 2, the solid **1**|SiO₂|TiO₂ catalyst was filtered from reaction mixture and additional substrate was added to the filtrate solution and a second reaction was performed. No new product formation or substrate consumption was observed after the second reaction showing that the active catalyst is not present in the reaction filtrate post reaction.

Table 2. Control Reactions Performed to Identify the Catalytically Active Species.

		
Rxn.	Catalyst	Yield ^a
1	1 SiO ₂ TiO ₂	90%
2	1 TiO ₂	32%
3	Reaction Filtrate	0%
4	Only SiO ₂	0%
5	Only TiO ₂	0%
6	1 nm TiO ₂ on SiO ₂	0%
7	1 mol% 1 + SiO ₂ <i>in situ</i>	0%
8	1 mol% 1 + TiO ₂ <i>in situ</i>	4%
9	1 mol% NiCl ₂ in solution	0%
10	1 mol% Rainey Ni in solution	1%
11	1 mol% NiCl ₂ + SiO ₂ <i>in situ</i>	0%
12	1 mol% Raney Ni + SiO ₂ <i>in situ</i>	0%
13	Ni nanoparticles SiO ₂ (CEDI)	1%
14	1 SiO ₂ TiO ₂ + Hg drop	82%

Conditions: 0.82 mmol phenylboronic acid, 0.68 mmol iodotoluene, 1.7 mmol K₃PO₄ in 20 ml 1:1 ethanol/water. 105 °C 24 hr. 0.9 mol% **1**|SiO₂|TiO₂, 1.1 mol% CEDI.

^aDetermined by GC-MS analysis.

To confirm the necessity of the **1**|SiO₂|TiO₂ structure, numerous other active catalysts were also considered. As indicated by reactions 4 and 5, the untreated metal oxides powders are not catalytically active for this cross-coupling transformation. SiO₂ ALD coated with TiO₂ without molecular nickel catalyst present was also not active (reaction 6). A mixture of homogenous molecular catalyst and fresh oxide particles, reactions 7 and 8, did not result in appreciable product formation, indicating that the ligand-first surface-attachment of the molecular catalyst is necessary in the hybrid design. Decomposition of the molecular nickel catalyst to nickel salts (NiCl₂) or metallic nickel during the reaction could have also been possible. Testing of NiCl₂ or metallic Rainey Ni both in solution and in the presence of oxide support (reactions 9 - 12) resulted in poor product yields (< 5%), indicating that these possible decomposition products are not responsible for the observed catalytic activity of **1**|SiO₂|TiO₂. We further examined the possibility that reduced nickel nanoparticles act as the catalytically active species. We synthesized 0.5 weight% nickel nanoparticle catalyst on the SiO₂ support using charge enhanced dry impregnation (CEDI).⁵⁸ The nickel nanoparticles did not exhibit catalytic activity in the water:ethanol mixture (rxn. 13),

further illustrating an advantage of the designed hybrid ALD catalyst. To test for possible advantageous metallic species being catalytically active, the hybrid ALD catalyst was exposed to the mercury drop test. Mercury is known to poison heterogeneous metal nanoparticle catalysts.⁵⁹ In the presence of Hg, the hybrid catalyst maintained catalytic activity (reaction. 13), which strongly indicates that the active catalytic species is molecular in nature. Furthermore, nickel first binding to the oxide surface to generate a SOMC moiety is highly unlikely, as SOMCs require extensive oxide surface preparation under air-free conditions,¹⁴ while **1**|SiO₂|TiO₂ was prepared in air without prior conditioning of the oxide surface.

A further summary of the reactivity and stability of **1**|SiO₂|TiO₂ in comparison to **1** and **1**|SiO₂ can be found in Table 3. The data in Table 3 supports the conclusion that the hybrid catalyst containing an ALD overcoating (**1**|SiO₂|TiO₂) exhibits increased Suzuki cross-coupling reactivity due to the construction of the catalyst leading to extended lifetimes for the molecular component of the catalyst. IR spectroscopy focusing on the carboxylic frequencies indicates prolonged binding of the ligand to the oxide surface only when the ALD overcoat is applied. In addition, ICPMS analysis of the catalyst and the reaction solution shows retention of the majority of the nickel on the solid catalyst with **1**|SiO₂|TiO₂. STEM-EDS analysis supports the ICPMS data, and elemental mapping (Figure S6) of **1**|SiO₂|TiO₂ post-reaction shows a uniform coating of the TiO₂ layer and well-dispersed nickel on the surface of the SiO₂ support. The characterization data in Table 3 combined with the reactivity data in Tables 1 and 2 provide compelling evidence that the designed hybrid catalyst **1**|SiO₂|TiO₂ is the catalytically active species for the test Suzuki cross-coupling reaction under the chosen conditions.

Table 3: Summary of the Characterization Data Comparing Homogeneous Catalyst (**1**), Hybrid Catalyst without ALD (**1**|SiO₂), and Hybrid Catalyst with ALD Overcoating (**1**|SiO₂|TiO₂).

		IR (COOH cm ⁻¹)		ICPMS (Ni wt%) catalyst		ICPMS (Ni) solution	EDS elements detected*		XRD (Ni particles?)	
Catalyst	%Yield	Pre	Post	Pre	Post	Post	Pre	Post	Pre	Post
1	0	1729	N/A	N/A	N/A	N/A	N/A	N/A	N/A	N/A
1 SiO ₂	5	1639	N.S.	0.35	0.06	170 µg	Ni	N.S.	No	No
1 SiO ₂ TiO ₂	90	1640	1640	0.35	0.31	35 µg	Ni, Ti	Ni, Ti, K, P	No	No

N/A: data not collected/not applicable. N.S.: no signal. Pre and Post refer to pre-reaction and post-reaction, reaction details in Table 1. *EDS detected Si and O in every measurement.

This hybrid catalyst exhibits desirable green chemistry principles^{48, 60} such as the use of earth abundant nickel, low metal loadings which help prevent product contamination,⁶¹ ease of catalyst separation from reaction mixtures without the need for column chromatography, and a green solvent mixture of H₂O and ethanol. To further evaluate the chemical stability of this catalysts design, **1**|SiO₂|TiO₂ was examined with X-ray emission spectroscopy (XES) before and after use in a Suzuki cross-coupling reaction. Figure 3 overlays the XES spectra at the Ni 2p emission for five different nickel samples. Here, the emission energy is indicative of the nickel's chemical binding state. The top two spectra are reference scans made on nickel metal and nickel oxide (NiO) powders. Here, we observe a clear shift in peak emission intensity from 8266.8 eV to 8267.5 eV, as would be expected for these reference powders' differences in chemical states. Next are scans for **1** in various states. First is the XES spectrum of **1**|SiO₂, the catalyst before ALD coating. This catalyst exhibits a peak intensity at 8268.0 eV. This peak intensity is 0.5 eV shifted from the oxide state, indicating that XES is capable of detecting the difference in chemical states between NiO and the molecular catalyst **1**. Shown next is the XES spectrum for **1**|SiO₂|TiO₂, which exhibits an identical peak emission energy to **1**|SiO₂ (8268.0 eV). This result again indicates that **1** maintains its molecular nature

after ALD coating. Lastly is the spectrum for the **1**|SiO₂|TiO₂ catalyst after a 24 hour reaction in 1:1 ethanol:water solvent. This “used” catalyst once again shows its maximum peak intensity at 8268.0 eV, further confirming Ni in **1** remains bound to its organic ligands. In fact, direct overlays of these three spectra, displayed in Figure S9, show that all three samples have nearly identical XES spectra. Furthermore, roughly 500 catalytic turnovers were achieved with **1**|SiO₂|TiO₂ for the reaction shown in Table 1, whereas the non-ALD catalyst **1**|SiO₂ was only able to achieve roughly 25 turnovers before deactivation (Figure S10).

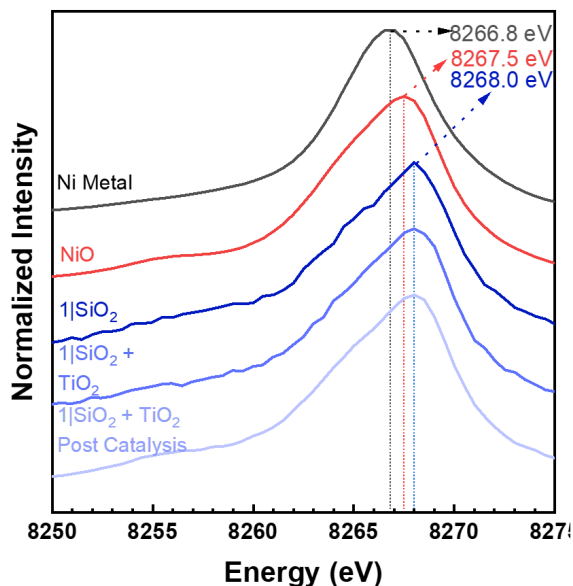


Figure 3. XES spectra overlays comparing the hybrid catalyst before ALD coating (**1**|SiO₂) to the hybrid catalyst after ALD before performing a cross-coupling reaction (**1**|SiO₂|TiO₂) and **1**|SiO₂|TiO₂ post catalytic reaction to nickel oxide and nickel metal samples supported on SiO₂ support.

To ensure this catalyst is generally amenable to Suzuki cross-coupling reactivity and not just applicable to a single reaction, a modest substrate scope for this catalyst was examined. Figure 4 shows the range of cross-coupling partners explored and products obtained from this hybrid ALD catalyst. In general, **1**|SiO₂|TiO₂ was able to couple a variety of aryl halide and aryl boronic acid substrates with yields that range between 49 to 90%. **1**|SiO₂|TiO₂ exhibits greater reactivity towards aryl iodides compared to aryl bromides or chlorides. This reactivity trend has been previously observed for [(2,2':6',2''-terpyridine)Ni(II)]Cl₂ cross-coupling catalysis.⁶² As can be seen in Figure 4, a range of electron donating and electron withdrawing substrates are amenable to cross-coupling using **1**|SiO₂|TiO₂ as the catalyst. This result illustrates that the reported hybrid catalyst motif may be a general approach towards designing cross-coupling catalysts.

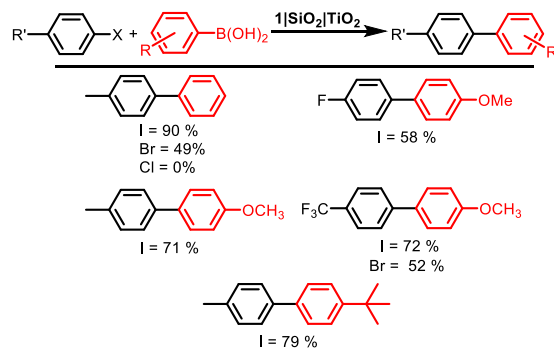


Figure 4. Catalytic Suzuki cross-coupling achieved by hybrid ALD catalyst. % yields are isolated yield and based on limiting reagent. 0.82 mmol phenylboronic acid, 0.68 mmol iodotoluene, 1.7 mmol K_3PO_4 in 20 ml 1:1 ethanol/water. 105 °C 24 hr. 100 mg $1[SiO_2]TiO_2$.

Conclusions

This study demonstrates a new paradigm in the design of hybrid catalysts in which ALD is used to improve the attachment and stability of molecular catalysts on solid metal oxide supports. Generating hybrid catalysts with increased catalyst lifetimes makes the catalysts amenable for the use of green solvents and easily separable from reaction solutions. At an optimal ALD layer thickness, the molecular catalyst remains highly active while still being resistant to surface detachment and subsequent deactivation. Through a series of control experiments and spectroscopic characterizations, we provide strong evidence for the active species to be the unperturbed molecular catalyst attached to the metal oxide surface and encased with an optimal ALD deposited TiO_2 layer. Interestingly, the exemplary molecular catalyst studied here is not catalytically active by itself in homogeneous solution for the target carbon-carbon cross-coupling reaction due to extremely short catalyst lifetimes. Thus, a combination of ligand-first surface attachment with molecular design and ALD application could lead to new approaches in catalyst discovery. Noteworthy here for green chemistry principles is that this hybrid catalyst was able to perform cross-coupling catalysis using a non-noble metal (nickel) and earth abundant oxides and is active in a near-neutral pH, primarily aqueous solution. Moreover, since the optimal ALD coating requires only about 10 reaction cycles, this process is technologically and economically viable for large-scale manufacturing.

Experimental

Materials: Compound **1** was synthesized according to previously reported procedures.⁶ $1[SiO_2]$ was prepared following the one-step method previously reported.⁶ Atomic layer deposition was carried out in a custom-built, hot-wall, flow-tube reactor with automated control software⁶³ using a $TiCl_4 + H_2O$ chemistry at 120 °C in a ~2 Torr flowing N_2 (>99.99% purity) atmosphere. ALD runs on catalyst powder were limited to a few grams sealed in a polyester fabric bag that permitted permeation of the precursor gases. To assist precursor gas permeation, a “hold” step was included in each ALD cycle. One full ALD cycle included: (1) close the gate valves, (2) pump down for 420 seconds, (3) reaction chamber isolation for 60 seconds, (4) $TiCl_4$ dose for 1 second directly into the isolated reaction chamber, (5) hold for 120 seconds, (6) pump down the reaction chamber for 30 seconds, (7) open the gate valves, (8) purge for 30 seconds, (9) H_2O dose

for 1 second, (10) purge for 30 seconds. The water dose, steps (9) and (10), were repeated three times for each cycle. Monitor silicon wafers were included in each run to estimate approximate TiO₂ film thickness using spectroscopic ellipsometry (Woollam Alpha-SE).⁶⁴ The procedure for the synthesis of Nickel nanoparticle catalysts prepared by charge enhanced dry impregnation (CEDI) has been reported.⁵⁸ The SiO₂ support is Aerosil 300 (Evonik) and is a fumed, amorphous silica with 300 m²/g surface area and an average particle size of ~ 20 nm. Cross-coupling reaction solutions were prepared with ultra-pure (18 MΩ) water and 200 proof ethanol. All other materials and supplies were used as received from the supplier unless otherwise noted.

Instrumentation: A Bruker Advance III HD 300 was used for NMR spectroscopy. ¹H data were collected at 300 MHz and ¹³C at 75 MHz. Bruker TopSpin software was used to process the NMR data. Inductively coupled plasma-mass spectrometry (ICP-MS) was collected on a Finnigan ELEMENT XR with a double focusing magnetic field with a quartz torch and injector (Thermo Fisher Scientific) and a 0.2 mL/min micromist U-series nebulizer (GE). Gas chromatography-mass spectrometry analyses were performed with a Shimadzu QP-20105 containing a RXI-5MS (Restek) column (30 m, 0.25 mm id). Mass spectrometer electron ionization was at 70 eV and the spectrometer was scanned from 1000 to 50 *m/z* at low resolution. Powder X-ray diffraction (XRD) was carried out with a Rigaku Miniflex-II with a D/teX Ultra silicon strip detector. Cu Kα radiation (λ = 1.5406 Å) was operated at 15 kV and 30 mA. Samples were loaded on a zero-background holder and scanned from 20-80° 2θ range at a scan rate of 3° 2θ/min. Fourier transform infrared-attenuated total reflection (FTIR-ATR) was performed on a Nicolet iS Fourier transform infrared spectrometer with an iD7 attenuated total reflectance attachment (diamond crystal). Before each sample set, a background scan of ambient atmosphere was collected and then subtracted from the experimental signal to calculate the final spectra reported. EPR spectra were collected on a Bruker EMXplus instrument equipped with a Bruker X-band microwave bridgehead. Spectra were recorded in a quartz EPR tube at room temperature at a power of 1.589 mW with a modulation amplitude of 2.0 G using the Xenon v1.1b.66 software. Nitrogen physisorption measurements were performed on samples pretreated for by placing the samples under 10 μmHg vacuum at room temperature, then ramping the temperature to 90 °C at 10 °C/minute and holding for 6 hours. Nitrogen physisorption measurements were collected at 77 K and surface area characterized by BET.

General Cross-Coupling Reaction Set Up: In a 50 mL round-bottom flask, 0.68 mmol aryl halide and 0.82 mmol of boronic acid were added to a 20 mL solution comprise of 1:1 ethanol: water. 1.7 mmol of K₃PO₄ and 0.1 g of **1**[SiO₂]/TiO₂ were added to the flask (unless otherwise stated in the manuscript). The solution was heated to 105 °C for 24 hours. The reaction was then allowed to cool to room temperature and the products were extracted with 3 rinses with pentane and purified by preparative scale TLC (90:10 pentane: ethyl acetate mobile phase). For catalyst recycling, the solid catalyst was gravity filtered from the reaction solution and rinsed three times with pentane and three times with ethanol and dried under a stream of N₂ (99.999%, Airgas) before being used in a new reaction.

Supporting Information: XRD data, EDS data, and ¹H and ¹³C NMR data.

Author Information:

Corresponding authors E-mails: vannucci@mailbox.sc.edu losego@gatech.edu

ORCID: Aaron K. Vannucci: [0000-0003-0401-7208](https://orcid.org/0000-0003-0401-7208)

ORCID: Mark D. Losego: [0000-0002-9810-9834](https://orcid.org/0000-0002-9810-9834)

Acknowledgments: This material is based upon work supported by the National Science Foundation under Grant Nos. [1954850] and [1954809].

References

1. B. Cornils and W. A. Herrman, Concepts in Homogeneous Catalysis: The Industrial View., *J. Catal.*, 2003, **216**, 23-31.
2. L. Duan, F. Bozoglian, S. Mandal, B. Stewart, T. Privalov, A. Llobet and L. Sun, A molecular ruthenium catalyst with water-oxidation activity comparable to that of photosystem II, *Nature Chem.*, 2012, **4**, 418-423.
3. P.-A. Payard, L. A. Perego, I. Ciofini and L. Grimaud, Taming Nickel-Catalyzed Suzuki-Miyaura Coupling: A Mechanistic Focus on Boron-to-Nickel Transmetalation, *ACS Catal.*, 2018, **8**, 4812-4823.
4. T. Inatomi, Y. Fukahori, Y. Yamada, R. Ishikawa, S. Kanegawa, Y. Koga and K. Matsubara, Ni(i)–Ni(iii) cycle in Buchwald–Hartwig amination of aryl bromide mediated by NHC-ligated Ni(i) complexes, *Catal. Sci. Tech.*, 2019, **9**, 1784-1793.
5. S. G. Rull, I. Funes-Ardoiz, C. Maya, F. Maseras, M. R. Frutos, T. R. Belderrain and M. C. Nicasio, Elucidating the Mechanism of Aryl Aminations Mediated by NHC-Supported Nickel Complexes: Evidence for a Nonradical Ni(0)/Ni(II) Pathway, *ACS Catal.*, 2018, **8**, 3733-3742.
6. R. J. Key, J. M. M. Tengco, M. D. Smith and A. K. Vannucci, A Molecular/Heterogeneous Nickel Catalyst for Suzuki–Miyaura Coupling, *Organometallics*, 2019, **38**, 2007-2014.
7. J. L. Fillol, Z. Codolà, I. Garcia-Bosch, L. Gómez, J. J. Pla and M. Costas, Efficient water oxidation catalysts based on readily available iron coordination complexes, *Nature Chem.*, 2011, **3**, 807-813.
8. U. J. Kilgore, J. A. S. Roberts, D. H. Pool, A. M. Appel, M. P. Stewart, M. R. DuBois, W. G. Dougherty, W. S. Kassel, R. M. Bullock and D. L. DuBois, [Ni(PPh₂NC₆H₄X₂)₂]²⁺ Complexes as Electrocatalysts for H₂ Production: Effect of Substituents, Acids, and Water on Catalytic Rates, *J. Am. Chem. Soc.*, 2011, **133**, 5861-5872.
9. S. Das, R. R. Rodrigues, R. W. Lamb, F. Qu, E. Reinheimer, C. M. Boudreaux, C. E. Webster, J. H. Delcamp and E. T. Papish, Highly Active Ruthenium CNC Pincer Photocatalysts for Visible-Light-Driven Carbon Dioxide Reduction, *Inorg. Chem.*, 2019, **58**, 8012-8020.
10. H. Shirley, X. Su, H. Sanjanwala, K. Talukdar, J. W. Jurss and J. H. Delcamp, Durable Solar-Powered Systems with Ni-Catalysts for Conversion of CO₂ or CO to CH₄, *J. Am. Chem. Soc.*, 2019, **141**, 6617-6622.
11. X. Cui, W. Li, P. Ryabchuk, K. Junge and M. Beller, Bridging homogeneous and heterogeneous catalysis by heterogeneous single-metal-site catalysts, *Nature Catal.*, 2018, **1**, 385-397.
12. A. K. Vannucci, L. Alibabaei, M. D. Losego, J. J. Concepcion, B. Kalanyan, G. N. Parsons and T. J. Meyer, Crossing the divide between homogeneous and heterogeneous catalysis in water oxidation, *Proc. Natl. Acad. Sci.*, 2013, **110**, 20918-20922.
13. N. T. S. Phan, M. Van Der Sluys and C. W. Jones, On the Nature of the Active Species in Palladium Catalyzed Mizoroki–Heck and Suzuki–Miyaura Couplings – Homogeneous or Heterogeneous Catalysis, A Critical Review, *Adv. Synth. Catal.*, 2006, **348**, 609-679.
14. C. Copéret, A. Comas-Vives, M. P. Conley, D. P. Estes, A. Fedorov, V. Mougél, H. Nagae, F. Núñez-Zarur and P. A. Zhizhko, Surface Organometallic and Coordination Chemistry toward Single-Site Heterogeneous Catalysts: Strategies, Methods, Structures, and Activities, *Chem. Rev.*, 2016, **116**, 323-421.
15. J. Lu, J. W. Elam and P. C. Stair, Synthesis and Stabilization of Supported Metal Catalysts by Atomic Layer Deposition, *Acc. Chem. Res.*, 2013, **46**, 1806-1815.

16. A. R. Mouat, A. U. Mane, J. W. Elam, M. Delferro, T. J. Marks and P. C. Stair, Volatile Hexavalent Oxo-amidinate Complexes: Molybdenum and Tungsten Precursors for Atomic Layer Deposition, *Chem. Mater.*, 2016, **28**, 1907-1919.
17. M. K. Samantaray, E. Pump, A. Bendjeriou-Sedjerari, V. D'Elia, J. D. A. Pelletier, M. Guidotti, R. Psaro and J.-M. Basset, Surface organometallic chemistry in heterogeneous catalysis, *Chem. Soc. Rev.*, 2018, **47**, 8403-8437.
18. J. Camacho-Bunquin, M. Ferrandon, H. Sohn, D. Yang, C. Liu, P. A. Ignacio-de Leon, F. A. Perras, M. Pruski, P. C. Stair and M. Delferro, Chemoselective Hydrogenation with Supported Organoplatinum(IV) Catalyst on Zn(II)-Modified Silica, *J. Am. Chem. Soc.*, 2018, **140**, 3940-3951.
19. Z. H. Syed, D. M. Kaphan, F. A. Perras, M. Pruski, M. S. Ferrandon, E. C. Wegener, G. Celik, J. Wen, C. Liu, F. Dogan, K. I. Goldberg and M. Delferro, Electrophilic Organoiridium(III) Pincer Complexes on Sulfated Zirconia for Hydrocarbon Activation and Functionalization, *J. Am. Chem. Soc.*, 2019, **141**, 6325-6337.
20. H. Tafazolian, D. B. Culver and M. P. Conley, A Well-Defined Ni(II) α -Diimine Catalyst Supported on Sulfated Zirconia for Polymerization Catalysis, *Organometallics*, 2017, **36**, 2385-2388.
21. D. B. Culver, H. Tafazolian and M. P. Conley, A Bulky Pd(II) α -Diimine Catalyst Supported on Sulfated Zirconia for the Polymerization of Ethylene and Copolymerization of Ethylene and Methyl Acrylate, *Organometallics*, 2018, **37**, 1001-1006.
22. J. D. A. Pelletier and J.-M. Basset, Catalysis by Design: Well-Defined Single-Site Heterogeneous Catalysts, *Acc. Chem. Res.*, 2016, **49**, 664-677.
23. R. J. Witzke, A. Chapovetsky, M. P. Conley, D. M. Kaphan and M. Delferro, Nontraditional Catalyst Supports in Surface Organometallic Chemistry, *ACS Catal.*, 2020, **10**, 11822-11840.
24. C. C. Malakar and G. Helmchen, Immobilized Catalysts for Iridium-Catalyzed Allylic Amination: Rate Enhancement by Immobilization, *Chem. Eur. J.*, 2015, **21**, 7127-7134.
25. Y.-B. Zhou, Z.-K. Liu, X.-Y. Fan, R.-H. Li, G.-L. Zhang, L. Chen, Y.-M. Pan, H.-T. Tang, J.-H. Zeng and Z.-P. Zhan, Porous Organic Polymer as a Heterogeneous Ligand for Highly Regio- and Stereoselective Nickel-Catalyzed Hydrosilylation of Alkyne, *Org. Lett.*, 2018, **20**, 7748-7752.
26. S. Kramer, N. R. Bennedsen and S. Kegnæs, Porous Organic Polymers Containing Active Metal Centers as Catalysts for Synthetic Organic Chemistry, *ACS Catal.*, 2018, **8**, 6961-6982.
27. F. M. Wisser, Y. Mohr, E. A. Quadrelli and J. Canivet, Porous Macroligands: Materials for Heterogeneous Molecular Catalysis, *ChemCatChem*, 2020, **12**, 1270-1275.
28. A. Dhakshinamoorthy, A. M. Asiri and H. Garcia, Formation of C-C and C-Heteroatom Bonds by C-H Activation by Metal Organic Frameworks as Catalysts or Supports, *ACS Catal.*, 2019, **9**, 1081-1102.
29. X. B. Chen, C. Li, M. Gratzel, R. Kostecki and S. S. Mao, Nanomaterials for renewable energy production and storage, *Chem. Soc. Rev.*, 2012, **41**, 7909-7937.
30. K. E. Dalle, J. Warnan, J. J. Leung, B. Reuillard, I. S. Karmel and E. Reisner, Electro- and Solar-Driven Fuel Synthesis with First Row Transition Metal Complexes, *Chem. Rev.*, 2019, **119**, 2752-2875.
31. D. L. Ashford, M. K. Gish, A. K. Vannucci, M. K. Brennaman, J. L. Templeton, J. M. Papanikolas and T. J. Meyer, Molecular Chromophore-Catalyst Assemblies for Solar Fuel Applications, *Chem. Rev.*, 2015, **115**, 13006-13049.
32. K. Hanson, M. K. Brennaman, A. Ito, H. L. Luo, W. J. Song, K. A. Parker, R. Ghosh, M. R. Norris, C. R. K. Glasson, J. J. Concepcion, R. Lopez and T. J. Meyer, Structure-Property Relationships in Phosphonate-Derivatized, Ru-II Polypyridyl Dyes on Metal Oxide Surfaces in an Aqueous Environment, *J. Phys. Chem. C*, 2012, **116**, 14837-14847.
33. A. K. Vannucci, Z. Chen, J. J. Concepcion and T. J. Meyer, Nonaqueous Electrocatalytic Oxidation of the Alkylaromatic Ethylbenzene by a Surface Bound RuV(O) Catalyst, *ACS Catal.*, 2012, **2**, 716-719.

34. Z. F. Chen, J. J. Concepcion, J. F. Hull, P. G. Hoertz and T. J. Meyer, Catalytic water oxidation on derivatized nanoITO, *Dalton Trans.*, 2010, **39**, 6950-6952.
35. K. L. Materna, R. H. Crabtree and G. W. Brudvig, Anchoring groups for photocatalytic water oxidation on metal oxide surfaces, *Chem. Soc. Rev.*, 2017, **46**, 6099-6110.
36. M. Opanasenko, P. Štěpnička and J. Čejka, Heterogeneous Pd catalysts supported on silica matrices, *RSC Advances*, 2014, **4**, 65137-65162.
37. S. Hübner, J. G. de Vries and V. Farina, Why Does Industry Not Use Immobilized Transition Metal Complexes as Catalysts?, *Adv. Synth. Catal.*, 2016, **358**, 3-25.
38. J. T. Hyde, K. Hanson, A. K. Vannucci, A. M. Lapidés, L. Alibabaei, M. R. Norris, T. J. Meyer and D. P. Harrison, Electrochemical Instability of Phosphonate-Derivatized, Ruthenium(III) Polypyridyl Complexes on Metal Oxide Surfaces, *ACS Appl. Mater. Inter.*, 2015, **7**, 9554-9562.
39. B. C. Vicente, Z. Huang, M. Brookhart, A. S. Goldman and S. L. Scott, Reactions of phosphinites with oxide surfaces: a new method for anchoring organic and organometallic complexes, *Dalton Trans.*, 2011, **40**, 4268-4274.
40. D. G. Brown, P. A. Schauer, J. Borau-Garcia, B. R. Fancy and C. P. Berlinguette, Stabilization of Ruthenium Sensitizers to TiO₂ Surfaces through Cooperative Anchoring Groups, *J. Am. Chem. Soc.*, 2013, **135**, 1692-1695.
41. M. D. Losego and K. Hanson, Stabilizing molecular sensitizers in aqueous environs, *Nano Energy*, 2013, **2**, 1067-1069.
42. S. Liu, J. M. Tan, A. Gulec, L. A. Crosby, T. L. Drake, N. M. Schweitzer, M. Delferro, L. D. Marks, T. J. Marks and P. C. Stair, Stabilizing Single-Atom and Small-Domain Platinum via Combining Organometallic Chemisorption and Atomic Layer Deposition, *Organometallics*, 2017, **36**, 818-828.
43. Z. Lu, R. W. Tracy, M. L. Abrams, N. L. Nicholls, P. T. Barger, T. Li, P. C. Stair, A. A. Dameron, C. P. Nicholas and C. L. Marshall, Atomic Layer Deposition Overcoating Improves Catalyst Selectivity and Longevity in Propane Dehydrogenation, *ACS Catal.*, 2020, **10**, 13957-13967.
44. S. Handa, E. D. Slack and B. H. Lipshutz, Nanonickel-Catalyzed Suzuki–Miyaura Cross-Couplings in Water, *Angew. Chem. Int. Ed.*, 2015, **54**, 11994-11998.
45. B. H. Lipshutz, When Does Organic Chemistry Follow Nature’s Lead and “Make the Switch”?, *J. Org. Chem.*, 2017, **82**, 2806-2816.
46. R. Jana, T. P. Pathak and M. S. Sigman, Advances in Transition Metal (Pd,Ni,Fe)-Catalyzed Cross-Coupling Reactions Using Alkyl-organometallics as Reaction Partners, *Chem. Rev.*, 2011, **111**, 1417-1492.
47. P. G. Gildner and T. J. Colacot, Reactions of the 21st Century: Two Decades of Innovative Catalyst Design for Palladium-Catalyzed Cross-Couplings, *Organometallics*, 2015, **34**, 5497-5508.
48. M. C. Bryan, P. J. Dunn, D. Entwistle, F. Gallou, S. G. Koenig, J. D. Hayler, M. R. Hickey, S. Hughes, M. E. Kopach, G. Moine, P. Richardson, F. Roschangar, A. Steven and F. J. Weiberth, Key Green Chemistry research areas from a pharmaceutical manufacturers’ perspective revisited, *Green Chem.*, 2018, **20**, 5082-5103.
49. J. Jo, Q. Tu, R. Xiang, G. Li, L. Zou, K. M. Maloney, H. Ren, J. A. Newman, X. Gong and X. Bu, Metal Speciation in Pharmaceutical Process Development: Case Studies and Process/Analytical Challenges for a Palladium-Catalyzed Cross-Coupling Reaction, *Organometallics*, 2019, **38**, 185-193.
50. K. Hanson, M. D. Losego, B. Kalanyan, G. N. Parsons and T. J. Meyer, Stabilizing Small Molecules on Metal Oxide Surfaces Using Atomic Layer Deposition, *Nano Lett.*, 2013, **13**, 4802-4809.
51. K. Hanson, M. D. Losego, B. Kalanyan, D. L. Ashford, G. N. Parsons and T. J. Meyer, Stabilization of [Ru(bpy)(2)(4,4'-(PO₃H₂)bpy)](2+) on Mesoporous TiO₂ with Atomic Layer Deposition of Al₂O₃, *Chem. Mater.*, 2013, **25**, 3-5.

52. D. H. Kim, M. D. Losego, K. Hanson, L. Alibabaei, K. Lee, T. J. Meyer and G. N. Parsons, Stabilizing chromophore binding on TiO₂ for long-term stability of dye-sensitized solar cells using multicomponent atomic layer deposition, *PCCP*, 2014, **16**, 8615-8622.
53. A. Winter and U. S. Schubert, Metal-Terpyridine Complexes in Catalytic Application – A Spotlight on the Last Decade, *ChemCatChem*, 2020, **12**, 2890-2941.
54. B. J. Brennan, M. J. Llansola Portolés, P. A. Liddell, T. A. Moore, A. L. Moore and D. Gust, Comparison of silatrane, phosphonic acid, and carboxylic acid functional groups for attachment of porphyrin sensitizers to TiO₂ in photoelectrochemical cells, *PCCP*, 2013, **15**, 16605-16614.
55. M. K. Nazeeruddin, R. Humphry-Baker, P. Liska and M. Gratzel, Investigation of sensitizer adsorption and the influence of protons on current and voltage of a dye-sensitized nanocrystalline TiO₂ solar cell, *J. Phys. Chem. B*, 2003, **107**, 8981-8987.
56. M. Norio and A. Suzuki, Palladium-Catalyzed Cross-Coupling Reactions of Organoboron Compounds, *Chem. Rev.*, 1995, **95**, 2457-2483.
57. N. A. DeLucia, A. Jystad, K. Vander Laan, J. M. M. Tengco, M. Caricato and A. K. Vannucci, A Silica Supported Molecular Palladium Catalyst for Selective Hydrogeoxygenation of Aromatic Compounds Under Mild Conditions, *ACS Catal.*, 2019, **9**, 9060-9071.
58. X. Zhu, H.-r. Cho, M. Pasupong and J. R. Regalbuto, Charge-Enhanced Dry Impregnation: A Simple Way to Improve the Preparation of Supported Metal Catalysts, *ACS Catal.*, 2013, **3**, 625-630.
59. K. C. Campbell and J. S. Hislop, Mercury adsorption, catalyst poisoning, and reactivation phenomena on metal catalysts, *J. Catal.*, 1969, **13**, 12-19.
60. P. T. Anastas and J. C. Warner, *Green Chemistry: Theory and Practice*, Oxford University Press, New York, 1998.
61. C.-J. Li and B. M. Trost, Green Chemistry for Chemical Synthesis, *Proc. Natl. Acad. Sci.*, 2008, **105**, 13197-13202.
62. A. Paul, M. D. Smith and A. K. Vannucci, Photoredox-Assisted Reductive Cross-Coupling: Mechanistic Insight into Catalytic Aryl–Alkyl Cross-Couplings, *J. Org. Chem.*, 2017, **82**, 1996-2003.
63. B. D. Piercy and M. D. Losego, Tree-based control software for multilevel sequencing in thin film deposition applications, *J. Vac. Sci. Technol., B*, 2015, **33**.
64. B. D. Piercy, C. Z. Leng and M. D. Losego, Variation in the density, optical polarizabilities, and crystallinity of TiO₂ thin films deposited via atomic layer deposition from 38 to 150 °C using the titanium tetrachloride-water reaction, *J. Vac. Sci. Tech. A*, 2017, **35**, 03E107.

TOC Graphic

